

激光功率对双激光束双侧同步焊接 TC4 钛合金 T 型接头断裂性能的影响机理

刘金钊, 颜廷艳, 康绪枫, 占小红*

南京航空航天大学材料科学与技术学院, 江苏 南京 211106

摘要 TC4 钛合金具有良好的综合力学性能,其激光焊接结构现已广泛应用于航空航天等领域。通过开展 TC4 钛合金双激光束双侧同步焊接试验,对不同激光功率下钛合金 T 型接头进行微观组织观察、Z 向拉伸试验以及断口观察。结果表明,激光功率的提高可显著增大接头的熔深、熔宽,激光功率为 2.1 kW 时,接头热影响区多为细小的等轴晶粒,当激光功率提高至 2.3 kW 时,下熔合线下部出现大面积粗晶区,部分晶粒尺寸超过了 100 μm 。此外,热输入的提高导致了接头焊缝区强度的降低,采用激光功率为 2.3 kW 的拉伸试样,其断裂面贯穿焊缝区域,断裂强度远低于采用较低功率的 1 号试样。断面微观形貌显示,激光功率较高时,试样断裂模式为韧性断裂与解离断裂组成的混合断裂。

关键词 激光技术; TC4 钛合金; 双激光束双侧同步焊接; 微观组织; 断裂性能

中图分类号 TG456.7; TG146.2+3

文献标志码 A

doi: 10.3788/CJL202148.1802007

1 引言

与传统结构材料钢、铝合金等相比,TC4 钛合金具有良好的比强度、比模量,优良的热强性以及耐腐蚀性^[1-3]。得益于其独特的性能优势,TC4 钛合金在航空航天领域的使用量得到日益增长。近年来,航空航天制造业对飞行器提出了大型化、轻量化等要求,减重成为飞行器制造首要的任务^[4-5]。蒙皮-桁条 T 型结构是大型飞行器常用的减重结构,目前,该结构的传统制造方法有铆接工艺以及单面焊双面成形工艺^[6]。然而,上述工艺在生产应用中均暴露出了不可忽视的问题,如减重效果差、蒙皮完整性遭到破坏等^[7]。

双激光束双侧同步焊接(DLBSW)是利用双激光束以一定角度同步作用在 T 型接头对称两侧的创新型制造工艺,它最先由空客公司提出,并于 2003 年实现了桁条壁板结构的批量化生产^[8]。作为一种创新型制造工艺,双激光束双侧同步焊接工艺既能获得成形美观、性能优异的 T 型接头,又能保证蒙皮的表面完整性,实现很好的变形控

制^[9-10]。目前,国内外学者已针对双激光束双侧同步焊接工艺展开了相关研究。余海松^[11]针对 5A90 铝锂合金双激光束双侧同步焊接工艺展开研究,并分析了工艺参数对接头的宏观形貌和微观组织的影响。Tao 等^[12]采用双激光束双侧同步焊接工艺焊接了 AA6156-T6 铝合金,并针对接头焊丝熔融行为以及焊接缺陷形成机理展开了研究。

由于 TC4 钛合金组织对热作用敏感,晶粒长大,驱动力高,焊接过程中热影响区的等轴晶粒受热循环作用极易粗化,从而形成较宽的过热区,进而削弱接头的综合力学性能和服役性能^[13-15]。因此,热输入的合理选择对钛合金双激光束焊接尤为重要。程广福^[16]针对 TC4 钛合金 TIG 焊接头粗晶区晶粒生长和组织转变进行了研究,发现接头热影响区粗晶区晶粒粗化严重,晶内为粗大针状 α' 相和残余 β 相。苏轩^[17]在 TC4 钛合金激光 MIG 复合焊研究中发现,多次焊接热循环将导致钛合金焊接接头抗拉强度变大,而抗冲击性能相对降低。

收稿日期: 2021-01-20; 修回日期: 2021-03-05; 录用日期: 2021-03-29

通信作者: *xiaohongzhan_nuaa@126.com

本文的研究目标为揭示激光功率对 TC4 钛合金 T 型接头微观组织的影响规律,进而探究显微组织对接头断裂性能的影响机理。首先,通过开展不同工艺参数下的 TC4 钛合金双激光束双侧同步焊接试验,获得成形良好的 T 型接头。针对 T 型接头开展微观组织研究以及 Z 向拉伸试验,分析不同激光功率下 TC4 钛合金 T 型接头的断裂机制。

2 试验材料及方法

2.1 试验材料

本文试验所选的蒙皮和桁条材料均为 TC4 钛合金 (Ti6Al4V),其化学成分与力学性能分别如表 1 和表 2 所示。此外,蒙皮、桁条厚度分别为 1.2 mm 和 2 mm,其中桁条两侧加工有 0.8 mm × 0.8 mm 的对称凸台,蒙皮-桁条结构具体尺寸如图 1(a)和图 1(b)所示。

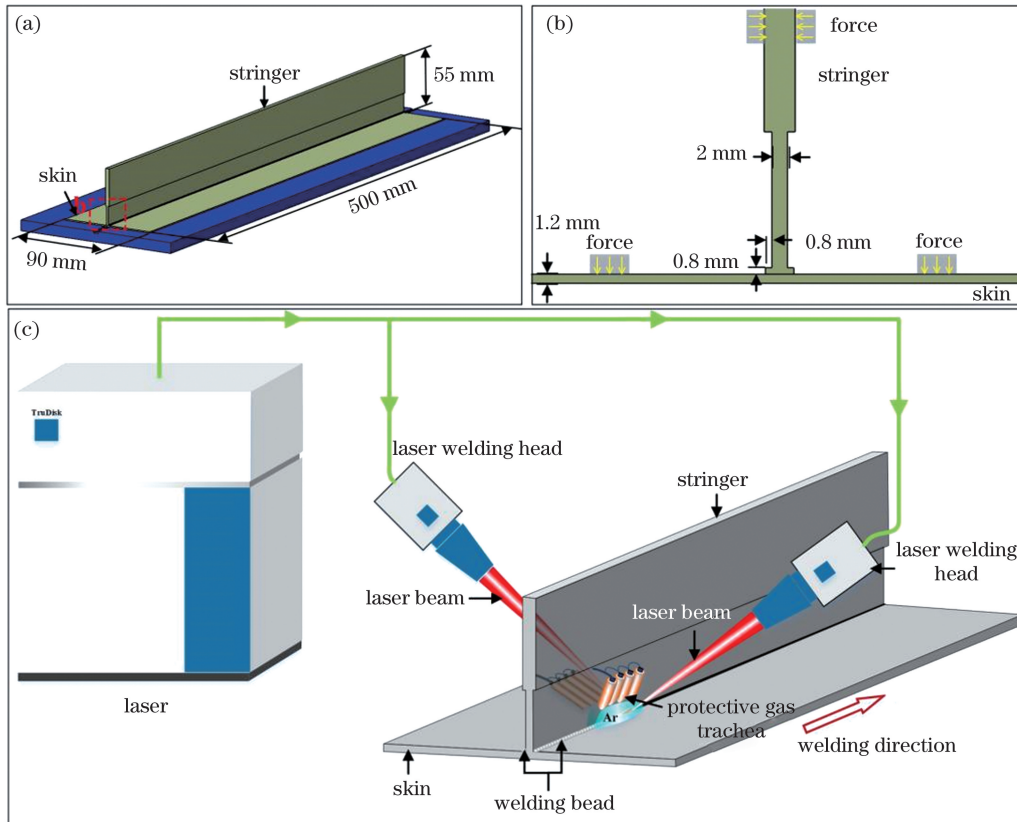


图 1 蒙皮-桁条结构尺寸及双激光束双侧同步焊接示意图。(a)(b)蒙皮-桁条结构尺寸示意图;(c)双激光束双侧同步焊接示意图

Fig. 1 Schematic diagrams of skin-stringer structure dimension and dual-laser-beam bilateral synchronous welding. (a)(b) Schematic diagrams of skin-stringer structure dimension; (c) schematic diagram of dual-laser-beam bilateral synchronous welding

表 1 TC4 钛合金化学成分

Table 1 Chemical composition of TC4 titanium alloy

unit: %

Composition	Fe	C	H	O	N	Al	V	Ti
Mass fraction	≤0.30	≤0.10	≤0.015	≤0.20	≤0.05	5.5-6.8	3.5-4.5	Bal.

表 2 TC4 钛合金力学性能

Table 2 Mechanical properties of TC4 titanium alloy

Material	Tensile strength /MPa	Yield strength /MPa	Elongation /%
Ti6Al4V alloy	895	835	8.2

2.2 试验方法

采用双激光束双侧同步焊接工艺对 TC4 钛合金蒙皮-桁条结构进行连接,其原理如图 1(c)所示,焊接过程中桁条两侧的激光束、保护气管需保持对称状态,预留凸台及部分蒙皮基材在激光束流作用

下熔化形成贯通熔池。本试验选用的激光器为德国通快公司生产的 TruDisk12003 碟片式激光器,通过两根光纤分别与两个激光焊接头相连;运动系统为两台倒挂 KR60HA 型 KUKA 机器人,焊接设备如图 2 所示。

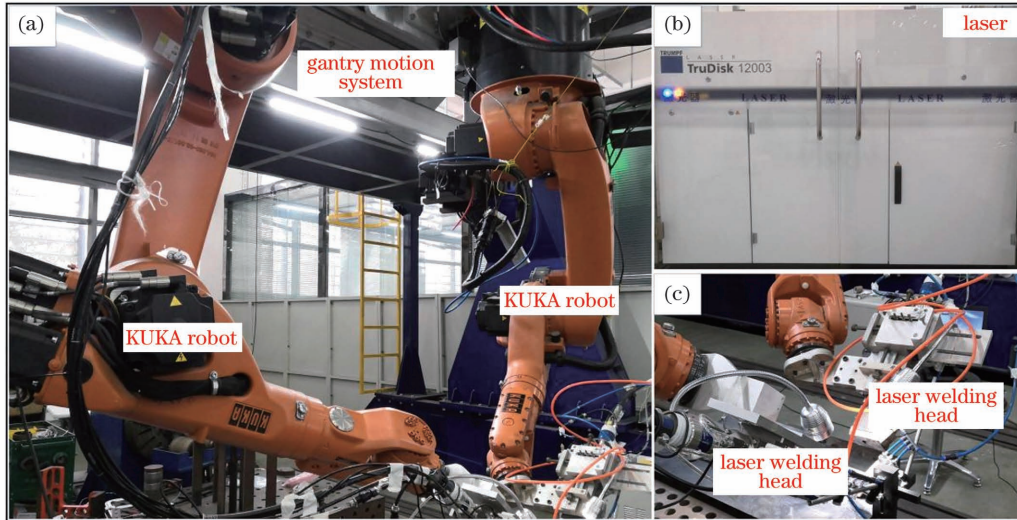


图 2 双激光束双侧同步焊接设备。(a)运动系统;(b)TruDisk 12003 激光器;(c)激光焊接头

Fig. 2 Equipment of DLBSW. (a) Motion system; (b) Trudisk 12003 laser; (c) laser welding head

为探究激光功率对焊接接头组织与力学性能的影响,本研究选取了成形良好的两组试板进行金相与拉伸试样制备,试验参数如表 3 所示。采用线切割取金相试样和拉伸试样,拉伸试样的选取位置和具体尺寸如图 3 所示。金相试样制备完成后,对

试样进行打磨、抛光和腐蚀,并在 MR-5000 型金相显微镜下观察接头显微组织。利用万能材料试验机开展室温下 T 型接头 Z 向拉伸性能测试,加载速率为 0.8 mm/min,拉伸试验结束后在扫描电子显微镜下观察断面形貌。

表 3 TC4 钛合金双激光束双侧同步焊接工艺试验参数

Table 3 Experimental parameters of DLBSW of TC4 titanium alloy

No.	Laser power / kW	Welding speed / (mm·s ⁻¹)	Laser incident angle / (°)	Defocus quantity / mm
1	2.1	22	40	0
2	2.3	22	40	0

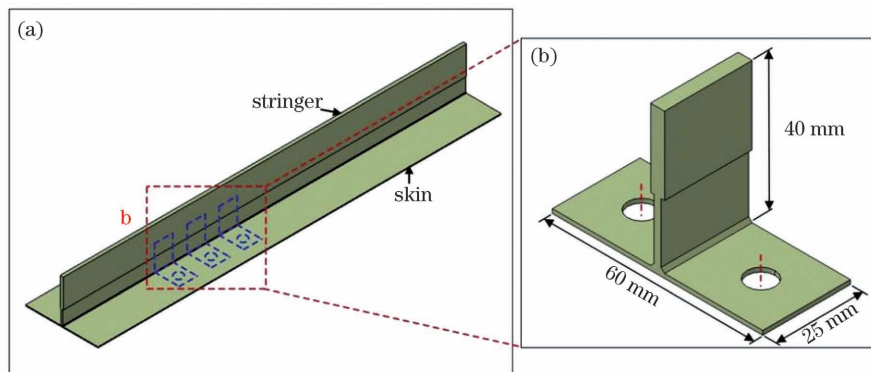


图 3 拉伸试样取样位置及尺寸。(a)拉伸试样取样位置;(b)拉伸试样尺寸

Fig. 3 Sampling position and dimension of the tensile specimen. (a) Sampling position of the tensile specimen; (b) dimension of the tensile specimen

3 试验结果和分析

3.1 焊缝宏观成形

图 4 为 TC4 钛合金双激光束双侧同步焊接焊缝

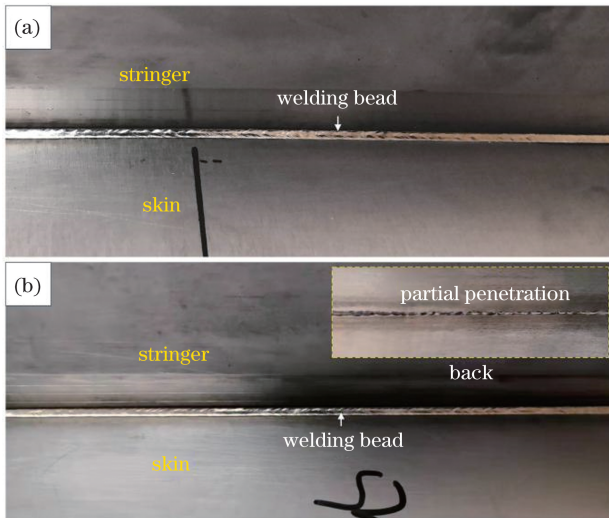


图 4 钛合金双激光束双侧同步焊接焊缝宏观成形情况。

(a) 1 号试样, $P=2.1$ kW; (b) 2 号试样, $P=2.3$ kW

Fig. 4 Macroscopical formation of the welding bead of

DLBSW. (a) No. 1 specimen, $P=2.1$ kW;

(b) No. 2 specimen, $P=2.3$ kW

缝宏观成形情况,由图可见,不同激光功率下焊缝正面的成形效果均良好,焊缝表面呈银白色,未出现氧化情况。观察蒙皮背面成形情况,可知当激光功率 P 为 2.1 kW 时,仍能保证蒙皮的表面完整性。然而,当激光功率提高至 2.3 kW 时,由图 4(b)可见,蒙皮背面出现局部焊透情况。

3.2 钛合金 T 型接头微观组织分析

图 5(a)和图 5(b)分别为 1 号金相试样焊接接头横截面和 2 号金相试样焊接接头横截面,图中 BM 为基材,HAZ 为热影响区,WB 为焊缝区, W_1 和 W_2 代表上熔宽, H_1 和 H_2 代表熔深。对比不同激光功率下 T 型接头横截面可知,随着激光功率的提高,上熔合线上部热影响区面积变化较小,而下熔合线下部的热影响区出现明显的扩展。上述现象说明,在双侧激光束作用下,熔池贯通,热量在熔池下部得到叠加,因此,激光功率的提高对熔合线附近母材晶粒再结晶的影响更加强烈。此外,对两组试样接头熔宽和蒙皮熔深进行测量,1 号试样熔宽和蒙皮熔深分别为 1.35 mm 和 0.85 mm,激光功率提高 200 W 后,2 号试样的熔宽达到了 1.92 mm,较 1 号试样提高了 42% ,其蒙皮熔深达到了 1.2 mm,即蒙皮完全焊透,与 1 号试样相比提高了 41% 。

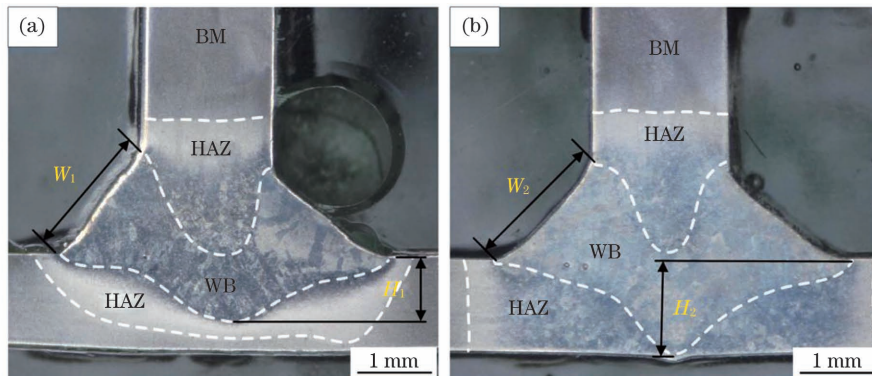


图 5 钛合金双激光束双侧同步焊接接头横截面。(a) 1 号试样, $P=2.1$ kW; (b) 2 号试样, $P=2.3$ kW

Fig. 5 Cross sections of titanium alloy DLBSW joint. (a) No. 1 specimen, $P=2.1$ kW; (b) No. 2 specimen, $P=2.3$ kW

图 6 为 1 号金相试样不同区域的微观组织形貌。由图 6(b)和图 6(c)可见,由于受到两侧熔融金属的热作用,上熔合区上部的热影响区可划分为明显的粗晶区(CGR)、细晶区(FGR)和过渡区(TR)。粗晶区为过度粗化的等轴晶粒,晶界内部析出贯穿整个晶粒的针状 α' 相,相比之下,细晶区晶粒粗化并不严重,且晶粒内部为短针状的 α' 相。此外,过渡区晶粒由于远离焊缝区且 TC4 钛合金热导率较低,受到的热作用较小,与母材相比,该区域带状组织消失,等轴晶粒长大程度有限。图 6(e)为下部焊

缝区组织,由图可见,焊缝区为粗大的原始 β 柱状晶,晶粒生长方向指向焊缝中心,由于焊缝区冷却速度较快,晶粒内部析出纵横交错的针状 α' 相。由图 6(d)和 6(f)可见,下熔合线下部为晶粒细小的过渡区,并未出现明显的粗晶区和细晶区。

图 7 为 2 号金相试样不同区域的微观组织形貌。如图 7(a)和图 7(b)显示,按晶粒长大程度,上熔合线上部仍可划分为粗晶区、细晶区和过渡区三个区域,但相比于 1 号试样,2 号试样的过渡区更窄,且过渡区晶粒较粗。图 7(d)为 2 号试样近上熔

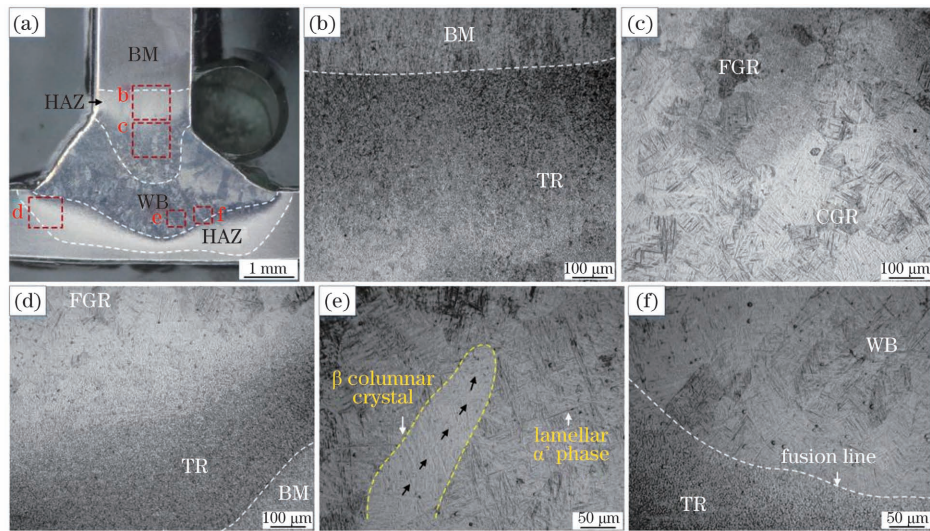


图 6 1 号试样接头不同区域微观组织。(a) 接头横截面; (b) 上部过渡区; (c) 上部细晶区、粗晶区; (d) 下部过渡区; (e) 焊缝区; (f) 下熔合线附近

Fig. 6 Microstructures in different regions of No. 1 specimen. (a) Joint cross section; (b) upper transition region; (c) upper fine grain region and coarse grain region; (d) lower transition region; (e) welding bead region; (f) near lower fusion line

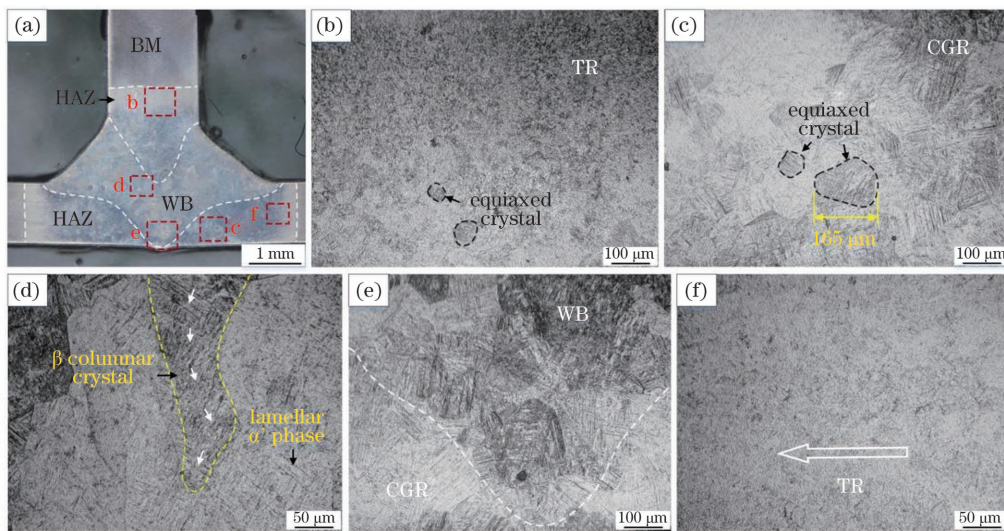


图 7 2 号试样接头不同区域微观组织。(a) 接头横截面; (b) 上部过渡区; (c) 上部细晶区、粗晶区; (d) 焊缝区; (e) 下熔合线附近; (f) 下部过渡区

Fig. 7 Microstructures in different regions of No. 2 specimen. (a) Joint cross section; (b) upper transition region; (c) upper fine grain region and coarse grain region; (d) welding bead region; (e) near lower fusion line; (f) lower transition region

合线焊缝区组织,由图可见,该区域为粗大的柱状晶组织,晶粒宽度在 $50 \sim 100 \mu\text{m}$ 左右,晶粒向下生长,且由于热输入的增大,晶粒内部析出的针状马氏体组织较 1 号试样发生明显的粗化。此外,与 1 号试样不同的是,由于激光功率的提高,2 号试样下熔合线下部出现明显的粗晶区、细晶区以及过渡区的划分。由图 7(c)和图 7(e)可见,下熔合区下方存在较宽的粗晶区,该区域晶粒受热作用发生严重粗化,部分等轴晶

粒尺寸达到了 $100 \mu\text{m}$,粗大等轴晶粒内部析出了针状 α' 相,过渡区较 1 号试样窄,且晶粒较粗。

3.3 钛合金 T 型接头力学性能分析

图 8 为不同激光功率下 TC4 钛合金 T 型接头的宏观断裂图,由图可见,当激光功率为 2.1 kW 时,裂纹首先在焊趾处形成,接头最终断裂位置位于两侧蒙皮,断面大致位于接头的热影响区。图 9 为 T 型接头 Z 向拉伸应力应变曲线,由图可见,1 号试

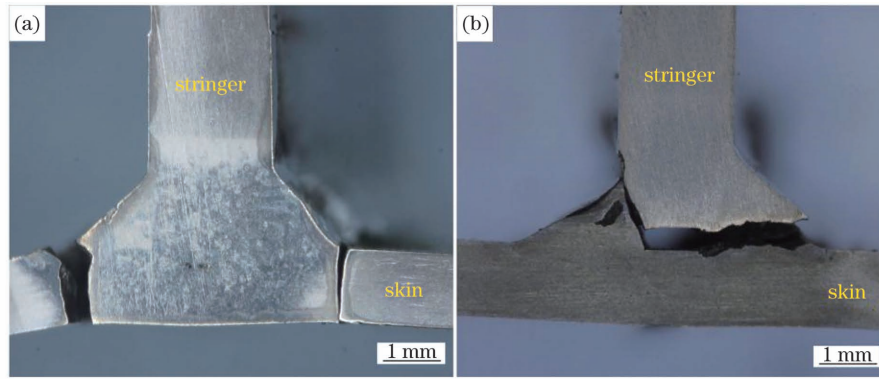


图 8 钛合金 T 型接头断裂宏观图。(a) 1 号试样, $P=2.1$ kW; (b) 2 号试样, $P=2.3$ kW

Fig. 8 Macro fracture diagrams of titanium alloy T-joint. (a) No.1 specimen, $P=2.1$ kW; (b) No.2 specimen, $P=2.3$ kW

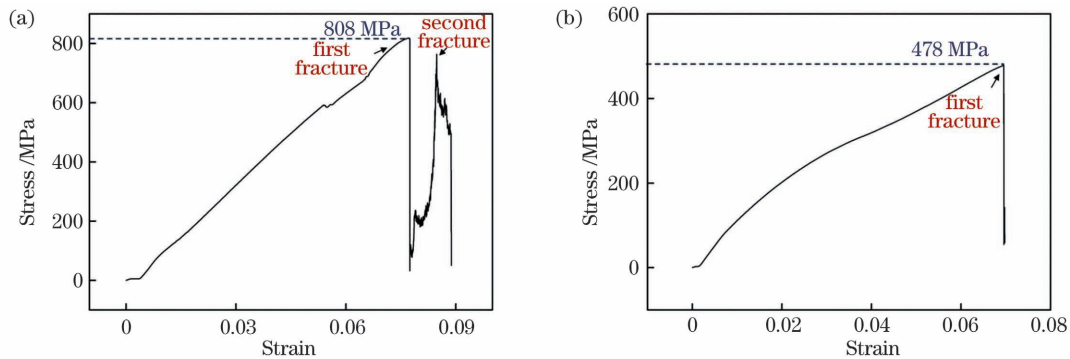


图 9 钛合金 T 型接头 Z 向拉伸应力-应变曲线。(a) 1 号试样, $P=2.1$ kW; (b) 2 号试样, $P=2.3$ kW

Fig. 9 Z-direction tensile stress-strain curves of titanium alloy T-joint. (a) No.1 specimen, $P=2.1$ kW; (b) No.2 specimen, $P=2.3$ kW

样在拉伸过程中发生了两次断裂,首次断裂强度超过了 800 MPa,达到了母材抗拉强度的 90%。当激光功率提高至 2.3 kW 时,由图 8(b)可见,2 号拉伸试样在焊缝区发生断裂,此时接头的断裂强度降低至 478 MPa。由此可推断,随着激光功率的增大,较高的焊接热量输入和较长的高温停留时间促进了焊

缝区相转变,导致该区域柱状晶内部析出的针状 α' 组织粗化,进而削弱了接头焊缝区的强度。

为探究激光功率对钛合金 T 型接头断裂模式的影响,分别对不同工艺参数获得的 T 型接头断面进行扫描电镜观察,如图 10 所示。激光功率为 2.1 kW 的 1 号试样断裂发生在接头蒙皮的热影响

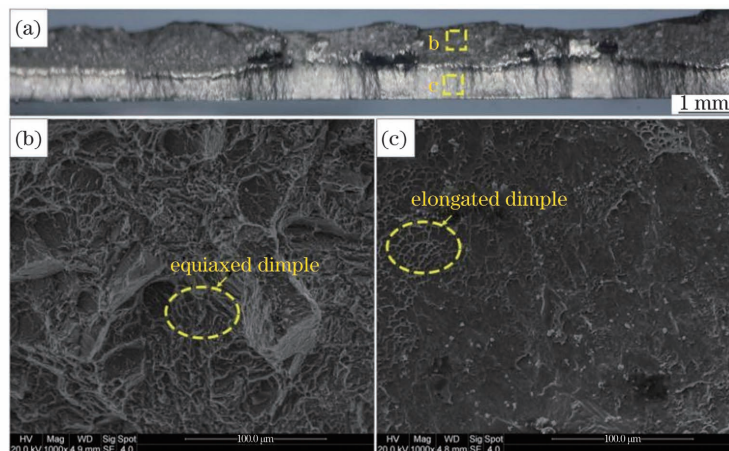


图 10 1 号试样断口微观形貌。(a)断口宏观形貌;(b)等轴韧窝;(c)拉长韧窝

Fig. 10 Macro and micro morphology of fracture surface of No. 1 sample. (a) Macro morphology of fracture surface; (b) equiaxed dimple; (c) elongated dimple

区,在拉伸过程中,接头同时受到拉应力和剪切应力的作用。由图 10(a)可见,断面可区分为明显的两部分,分界上方呈灰暗色,图 10(b)显示该区域为等轴韧窝。分析其原因可知,初期裂纹主要以微孔形核、长大、破裂的形式扩展,微孔破裂后即形成深度较大的等轴韧窝。随着应力在裂纹尖端的集中,裂纹扩展速率增大,微孔形核后来不及长大,在断裂过程中被拉长,最终在断面上形成具有一定走向的拉长韧窝,如图 10(c)所示。由此可判断 1 号试样的断裂模式为微孔聚集型断裂,亦属于韧性断裂。

当激光功率提高至 2.3 kW 时,2 号试样断裂发生在焊缝区域,对比图 11(a)和图 11(b)可见,断面为混合形貌,除图 11(a)所示的等轴韧窝外,在接头

断面上可以找到针状 α' 相剥离界面,因此可判断接头断裂模式为韧性断裂与解离断裂组成的混合断裂。形成上述现象的原因为:针状 α' 相属于硬质相。图 11(d)所示的能谱测试(EDS)结果显示其内部固溶有大量的 α 相,形成元素铝(Al)和钒(V),强烈的固溶强化作用使得 α' 相不易产生变形和断裂。同时,激光功率的提高引起焊缝区针状 α' 相粗化严重,削弱了相界面的连接,最终在试样断裂过程中导致针状 α' 相被近乎完整地剥离。此外,由图 11(c)可清晰地看到断裂面上存在多个破裂的气孔缺陷,在断裂过程中气孔缺陷将作为裂纹源进一步促进裂纹的扩展,这也是 2 号试样断裂强度降低的另一原因。

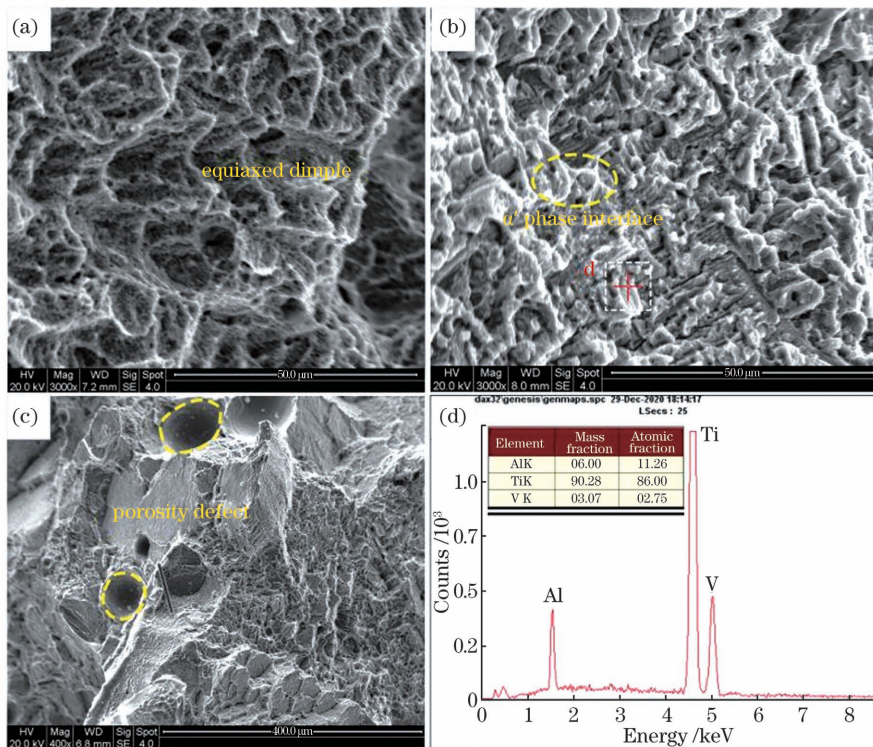


图 11 2 号试样断面宏微观形貌。(a)等轴韧窝;(b)剥离 α' 相界面;(c)气孔缺陷;(d)EDS 结果

Fig. 11 Macro and micro morphology of fracture surface of No. 2 sample. (a) Equiaxed dimples; (b) exfoliated α' phase interface; (c) porosity defects; (d) EDS results

4 结 论

针对 TC4 钛合金双激光束双侧同步焊接接头微观组织和 Z 向拉伸性能进行了研究,分析了不同激光功率对 T 型接头断裂性能的影响机理。可得到以下结论:

1) 随着激光功率的增大,TC4 钛合金 T 型接头横截面的熔宽和蒙皮熔深显著增大,与激光功率 2.1 kW 下的接头形貌相比,采用 2.3 kW 时接头熔

深、熔宽均增大约 40%。

2) TC4 钛合金双激光束焊接 T 型接头对激光功率的改变较为敏感,采用较高激光功率时,下熔合线下部的热影响区将出现大面积的粗晶区,部分晶粒尺寸达到了 100 μm ;相反,激光功率为 2.1 kW 时,下熔合线下部为较宽的过渡区,粗晶区和细晶区并不明显。

3) 1 号拉伸试样断裂发生在蒙皮热影响区,其断裂强度超过了母材强度的 90%;当激光功率提高

至 2.3 kW 时,2 号拉伸试样断裂在焊缝区,其强度较 1 号试样显著降低。

4) 由 T 型接头断裂的宏微观图观察可知,当激光功率为 2.1 kW 时,1 号拉伸试样的断裂模式为微孔聚集型断裂,属于韧性断裂。当激光功率提高至 2.3 kW 后,2 号拉伸试样断面为等轴韧窝与剥离 α' 相界面组成的混合形貌,其断裂模式为韧性断裂与解离断裂组成的混合断裂。

参 考 文 献

- [1] Qi Z J, Zhang X X, Wang Y Y, et al. Effect of B on microstructure and tensile properties of laser additive manufactured TC4 alloy [J]. Chinese Journal of Lasers, 2020, 47(6): 0602002.
齐振佳, 张晓星, 王豫跃, 等. 硼对激光增材制造 TC4 微观组织及力学性能的影响 [J]. 中国激光, 2020, 47(6): 0602002.
- [2] Akman E, Demir A, Canel T, et al. Laser welding of Ti_6Al_4V titanium alloys [J]. Journal of Materials Processing Technology, 2009, 209(8): 3705-3713.
- [3] Qiu Y, Zhang F Y, Hu T T, et al. Effect of laser power on microstructure and hardness of Ti40 flame-retardant titanium alloy deposited by laser cladding on TC4 surface [J]. Chinese Journal of Lasers, 2019, 46(11): 1102011.
邱莹, 张凤英, 胡腾腾, 等. 激光功率对 TC4 表面熔覆 Ti40 阻燃钛合金组织及硬度的影响 [J]. 中国激光, 2019, 46(11): 1102011.
- [4] Ouyang Z P. Study on the stability of dual laser-beam bilateral synchronous welding for T-structure of aluminium alloys [D]. Nanjing: Nanjing University of Aeronautics and Astronautics, 2012.
欧阳自鹏. 铝合金 T 型接头双激光束双侧同步焊接稳定性研究 [D]. 南京: 南京航空航天大学, 2012.
- [5] Cui L, Yang X Q, Xie Y H, et al. Process parameter influence on defects and tensile properties of friction stir welded T-joints on AA6061-T4 sheets [J]. Materials & Design, 2013, 51: 161-174.
- [6] Zhan X H, Zhao Y Q, Chen S, et al. Research progress on double laser-beam bilateral synchronous welding of T-joints for light alloy [J]. Aeronautical Manufacturing Technology, 2020, 63(11): 20-31.
占小红, 赵艳秋, 陈帅, 等. 轻合金 T 型结构双激光束双侧同步焊接技术研究进展 [J]. 航空制造技术, 2020, 63(11): 20-31.
- [7] Zhao Y, Zhou L L, Wang Q Z, et al. Defects and tensile properties of 6013 aluminum alloy T-joints by friction stir welding [J]. Materials & Design, 2014, 57: 146-155.
- [8] Ma X Y, Gong S L, Zhang J X, et al. Influence of the welding conditions on weld defects in double-sided laser beam welded T-joints of Ti-6Al-4V alloy [J]. Chinese Journal of Lasers, 2016, 43(2): 0203006.
马旭颐, 巩水利, 张久兴, 等. 焊接参数对 Ti-6Al-4V 合金双侧同步激光焊接 T 型接头缺陷的影响 [J]. 中国激光, 2016, 43(2): 0203006.
- [9] Zheng W J. Numerical simulation of bilateral synchronous laser beam welding for T-joint of aluminum alloys [D]. Harbin: Harbin Institute of Technology, 2011.
郑文健. 铝合金 T 型接头双束激光双侧同步焊接的数值模拟研究 [D]. 哈尔滨: 哈尔滨工业大学, 2011.
- [10] Yang Z B, Tao W, Li L Q, et al. Double-sided laser beam welded T-joints for aluminum aircraft fuselage panels: process, microstructure, and mechanical properties [J]. Materials & Design, 2012, 33: 652-658.
- [11] Yu H S. Thermo-mechanical coupling analysis of dual laser beam bilateral welding for Al-Li alloy skin-stringer structure [D]. Nanjing: Nanjing University of Aeronautics and Astronautics, 2019.
余海松. 铝锂合金蒙皮桁条结构双激光束双侧焊接热机耦合分析 [D]. 南京: 南京航空航天大学, 2019.
- [12] Tao W, Yang Z B, Chen Y B, et al. Double-sided fiber laser beam welding process of T-joints for aluminum aircraft fuselage panels: filler wire melting behavior, process stability, and their effects on porosity defects [J]. Optics & Laser Technology, 2013, 52: 1-9.
- [13] Fu P F, Mao Z Y, Zuo C J, et al. Microstructures and fatigue properties of electron beam welds with beam oscillation for heavy section TC4-DT alloy [J]. Chinese Journal of Aeronautics, 2014, 27(4): 1015-1021.
- [14] Kashaev N, Ventzke V, Fomichev V, et al. Effect of Nd: YAG laser beam welding on weld morphology and mechanical properties of Ti-6Al-4V butt joints and T-joints [J]. Optics and Lasers in Engineering, 2016, 86: 172-180.
- [15] Gu X Y, Zhu K X, Sui C L, et al. Control of microstructure and property of pulse laser welded joint of magnesium/titanium alloy [J]. Chinese Journal of Lasers, 2020, 47(1): 0102005.
谷晓燕, 朱开轩, 隋成龙, 等. 镁合金/钛合金脉冲激光焊接头的组织、性能调控 [J]. 中国激光, 2020, 47(1): 0102005.
- [16] Cheng G F. Grain growth and microstructure transformation in the heat affect zone of gas tungsten arc welding of fine grain TC4 alloy [D]. Harbin: Harbin Institute of Technology, 2008.

程广福. 细晶粒 TC4 钛合金 TIG 焊 HAZ 晶粒长大及组织转变规律 [D]. 哈尔滨: 哈尔滨工业大学, 2008.

[17] Su X. Characteristics of medium thickness of

titanium plate laser-MAG hybrid welding [D]. Harbin: Harbin Institute of Technology, 2014.

苏轩. 中厚度钛合金激光-MIG 复合焊接特性研究 [D]. 哈尔滨: 哈尔滨工业大学, 2014.

Influence of Laser Power on Fracture Properties of TC4 Titanium Alloy T-Joint Manufactured Using Dual-Laser-Beam Bilateral Synchronous Welding

Liu Jinzhao, Yan Tingyan, Kang Xufeng, Zhan Xiaohong*

College of Materials Science and Technology, Nanjing University of Aeronautics and Astronautics, Nanjing, Jiangsu 211106, China

Abstract

Objective In recent years, the aerospace manufacturing industry has proposed the requirements for large-scale and lightweight aircraft, and weight reduction has become the first priority of the aircraft manufacturing industry. Dual-laser-beam bilateral synchronous welding (DLBSW) is an innovative manufacturing process for producing the skin-stringer T-shaped structure, which was first proposed by Airbus. Currently, the study of DLBSW has mainly focused on the skin-stringer T-joints of aluminum alloy, with only a few references to the Ti_6Al_4V alloy T-joints and their properties. This T-joint forms a molten pool under the action of bilateral laser beams during the process of DLBSW, and the thermal effect is superimposed at the bottom of the molten pool. Because the Ti_6Al_4V alloy is sensitive to thermal action, the equiaxial grain in the heat-affected zone (HAZ) is easily coarsened during welding, which weakens the mechanical properties and service performance of the T-joint. Therefore, a rational selection of heat input is necessary for the laser welding of the titanium alloy. This study aims to reveal the influence of laser power on the microstructure of the Ti_6Al_4V alloy T-joint and explore the influence of microstructure on the fracture performance of the joint.

Methods In this study, the DLBSW experiment of the Ti_6Al_4V alloy T-joints was performed using two KUKA robots and a TruDisk 12003 laser produced by TRUMPF. The laser and the laser welding head are connected by two optical fibers. During the welding process, the laser beam and shielding gas were delivered symmetrically along the center line of the stringer (Fig. 1). Following the welding experiments, two groups of well-formed T-joints were selected for metallographic and tensile specimen preparation. The specimens were cut along the cross-section of T-joints, and the uneven area is avoided. The microstructure of the joint after polishing and corrosion was observed under an MR-5000 metallographic microscope. The tensile experiment was performed using an electromechanical universal testing machine at 25 °C. The loading rate was set to 0.8 mm/min, and the fracture morphology was observed using a scanning electron microscope.

Results and Discussions When the laser power is 2.1 kW, the HAZ above the upper fusion zone of the joint can be divided into the obvious coarse grain region (CGR), fine grain region (FGR), and transition region (TR) owing to the thermal effect of the molten metal on both sides of specimen. There is a large area of TR below the lower fusion zone without the obvious CGR and FGR (Fig. 6). The fracture surface of the joint is near the HAZ, and the tensile strength exceeds 800 MPa (Fig. 8). When the laser power is 2.3 kW, the α' phase that precipitated inside the columnar crystal in the weld bead zone coarsenes significantly because of the increase in heat input. Additionally, different from the joint adopting laser power of 2.1 kW, the HAZ below the lower fusion zone of joint No.2 can be divided into the CGR, FGR, and TR owing to the increase in laser power. A wide CGR appears below the lower fusion zone, where the grains have severely coarsened and some of the equiaxed grains have increased to 100 μm in size (Fig. 7). The joint is invalid in the weld bead zone, and the tensile strength is only 478 MPa (Fig. 8). The fractographs of the joint are mixed, except for the equiaxed dimples, and the exfoliated lamellar α' phase interface can be found on the fracture surface. It can be concluded that the fracture mode of specimen No.3 is a hybrid

fracture, comprising both the cleavage and ductile fractures (Fig. 11).

Conclusions Experimental results indicate that the $\text{Ti}_6\text{Al}_4\text{V}$ alloy T-joint manufactured by DLBSW is more sensitive to changes in the laser power. When the laser power increases, a large area of CGR is observed below the lower fusion zone, with some grain size reaching $100\ \mu\text{m}$. However, the region below the lower fusion zone of the joint adopting the laser power of 2.1 kW is a wider TR, while those of the CGR and FGR are not obvious. The joint under the laser power of 2.1 kW failed in the HAZ on the skin when a higher tensile strength exceeded 90% of the strength of the base material. When the laser power is increased to 2.3 kW, the joint is fractured in the weld bead zone, and its strength is significantly reduced compared with the specimen adopting a laser power of 2.1 kW. According to the fractographs of the joint, the fracture mode of the joint under lower laser power is a microporous aggregation fracture, which is classified as a ductile fracture. When the laser power is increased to 2.3 kW, the fracture mode of the joint is a combination of the ductile and cleavage fractures, with a mixed morphology comprising equiaxed dimples and exfoliated lamellar α' phase interface.

Key words laser technology; TC4 titanium alloy; dual-laser-beam bilateral synchronous welding; microstructure; fracture properties

OCIS codes 140.3590; 140.6810; 140.3390